Toward Graphene#Enhanced Spectroelectrochemical Sensors

ADVANCED MATERIALS INTERFACES
www.advmatinterfaces.de

Toward Graphene-Enhanced Spectroelectrochemical Sensors

*Preeti Kaushik, Farjana J. Sonia, Golam Haider, Mukesh Kumar Thakur, Václav Valeš, Jing Kong, and Martin Kalbáč**

Spectroelectrochemical sensors (SPECSs) sensitive to the least amount of sample are crucial for widespread applications, including early-stage detection of fatal diseases and other biomedical applications. However, despite the major disadvantage of biomolecule instability on noble metal nanoparticle-assisted surface-enhanced SPECSs, designing a suitable alternative remains a great challenge. The authors report a proof-of-concept graphene-enhanced spectroelectrochemical sensors (GE-SPECSs) employing graphene-enhanced Raman spectroscopy (GERS). Pristine (p-) and hydrogenated (h-) single-layer graphene (SLG) are utilized to study the oxidized and reduced states of a probe molecule, methylene blue (MB). The hole-doped h-SLG possesses efficient GERS signals compared with p-SLG, resulting in a limit of detection (LOD) < 10^{-7} M. By taking advantage of the tunable work function of graphene, the authors demonstrate that the GERS signal from the probe molecule can be varied and different oxidation states of the molecule can be studied by applying suitable external potentials. The LOD obtained in an aqueous system (≈10^{-7} M) is comparable with standard surface-enhanced SPECSs. The authors' design thus creates a novel pathway for developing highly efficient, biofriendly, and cost-effective SPECSs.

1. Introduction

Raman spectroscopy is one of the most powerful, simple, and non-destructive techniques for identifying chemical species and structures of materials. The Raman scattering cross section is low (10–30 cm^2 $molecule^{-1}$), and the scattered intensity of Raman modes is weak, resulting in low sensitivity. Over the years, several methods to enhance Raman scattering intensity have been reported, and surface-enhanced Raman scattering (SERS) became the most conventional technique for probing molecules at the lower detection limit.[1,2] The SERS effect arises mainly from electromagnetic (EM) and chemical (CM) enhancement of the Raman signal.[3] The EM enhancement is on the order of $\approx|E|^4$, amplifying signals $>10^8$, where E is the intensity of the EM field. On the other hand, CM enhancement has been shown to enhance the signal ≈10–100×. Nevertheless, SERS enhancement is contingent on the quality of the substrate. Preparation of a suitable substrate requires rigorous micro/nanofabrication processes, such as electrochemical or high vacuum deposition of noble metals (e.g., Ag, Au, Cu) or the self-assembly of size-controlled colloidal noble metal nanoparticles, which are very complex, contaminated, and not homogenous, leading to a lowered SERS effect. Moreover, when metal-based rough substrates, such as Ag or Cu, are used for SERS, they tend to oxidize, which prevents their use in some applications. Additionally, noble metals have relatively poor biological compatibility, hindering their use in biomedical applications.

Recently, graphene-enhanced Raman spectroscopy (GERS) has emerged as a novel technique where graphene-based ultra-smooth substrates exhibit strong Raman enhancement from adsorbed molecules.[4–6] Graphene is cheap, easy to produce, and remains stable even in relatively harsh conditions. The flat and chemically inert surface and environmentally friendly nature of graphene make it compatible for widespread use including biosensing, biomedical, and environmental applications.[7–9] The GERS technique is associated with the CM enhancement mechanism, where the charge transfer occurs between adsorbed molecules and the substrate.[4,10] As the surface plasmon on graphene is in the terahertz range rather than the visible range, graphene does not support EM enhancement by the excitation of visible energy photons.[11] Chemical mechanism-initiated GERS facilitates molecular selectivity, enhancing the charge transfer between the molecules and the graphene. The high stability and reproducibility of the Raman enhanced spectra from graphene makes GERS more suitable for applications than SERS.[12] It has been previously reported that the enhancement from GERS on nitrogen-doped graphene was about ten times higher than SERS with the same probe molecules, while for pristine graphene, it was five times higher.[13] Different molecules have been probed with GERS, making it an effective approach for sensing.[14,15] Theoretical and experimental studies have been conducted to obtain more insight into the mechanism

P. Kaushik, F. J. Sonia, G. Haider, M. K. Thakur, V. Valeš, M. Kalbáč
J. Heyrovský Institute of Physical Chemistry
Czech Academy of Sciences
Dolejškova 2155/3, Prague 18200, Czechia
E-mail: kalbac@jh-inst.cas.cz
J. Kong
Department of Electrical Engineering and Computer Science
Massachusetts Institute of Technology
77 Massachusetts Avenue, Cambridge, MA 02139, USA

The ORCID identification number(s) for the author(s) of this article can be found under https://doi.org/10.1002/admi.202200478.

DOI: 10.1002/admi.202200478

for GERS.[16,17] Barros et al. have shown that an enhanced Raman signal arises when the excitation energy of the laser is comparable to the energy difference between the Fermi energy of graphene and the energy of the highest occupied molecular orbital (HOMO)/lowest unoccupied molecular orbital (LUMO) states of the molecule. In support of this theory, Huang et al. later determined the dependence of Raman scattering on the HOMO/LUMO levels of a molecule with respect to the Fermi energy of graphene.[18] Thus, GERS enhancement is selective to specific molecules that fulfil the above criterion. Quite recently, we have shown different GERS enhancements utilizing chemically modified graphene, which have different levels of doping.[19] However, graphene possesses a tunable work function with the application of external potential.[20] Utilizing this property, an electrochemical GERS sensor has huge potential to circumvent the rigid energy-specific basis of the enhancement.

Partial hydrogenation of graphene is an effective route for engineering the electronic structure, tailoring the chemical properties and making it a functional material for electronic and optical applications.[21–23] The electrochemical properties of hydrogenated graphene have been investigated by Poh et al.[24,25] In a gated field-effect transistor configuration Jiang et al. have observed that electron transfer rate could be controlled by changing the density of hydrogen atoms on the graphene.[25] However, the electrochemical doping of hydrogenated graphene through in situ Raman measurements has not yet been explored, where resonant charge transfer of a probe molecule on graphene could be spectroscopically studied applying a suitable electrochemical potential.

Methylene blue (MB), a cationic water-soluble dye, serves as a catalyst and is used in different applications, such as clinical and chemical treatments, as a dying agent, electrochemical sensors, and biosensors.[26–29] Additionally, MB, a redox probe, has been studied for its electrochemical activity and as an electron transfer mediator.[30–32] Graphene oxide and MB-based nanocomposites have been investigated for their biosensing activity.[33,34] MB dye has been a well-known probe molecule to investigate SERS strength of metallic nanoparticle based substrates.[2,35–38] Hao et al. have investigated GERS signal of MB showing significant influence of applied electric field and chemical doping on graphene, where a higher effect due to chemical doping than field-effect was observed.[39] Furthermore, it has been shown that doped graphene exhibited improved Raman enhancement of MB for detecting low concentrations.[13] Recently, Kaya et al. have observed that MB molecules bind strongly to chemical vapor deposition (CVD) graphene through electrostatic π–π interactions without forming a covalent bond.[40] Thus, MB can serve as an excellent probe material for demonstrating graphene-enhanced spectroelectrochemical sensor (GE-SPECS).

This study demonstrates an electrochemical GERS sensor utilizing pristine (p-) and hydrogenated (h-) single layer graphene (SLG), using MB as a probe molecule. We observed that hole-doped h-SLG provides greater GERS signals than p-SLG, resulting in a limit of detection (LOD) $\approx 10^{-7}$ M. By electrochemically tuning the work function of graphene, it was found that the GERS signal can be adjusted, and different oxidation states of the molecule can be studied by applying a suitable external potential. The obtained overall LOD $\approx 10^{-7}$ M in an aqueous system is comparable with standard surface-enhanced spectroelectrochemical sensors based on noble metal nanoparticles.

2. Results and Discussion

First, we investigated the spectroelectrochemical behavior of p-SLG and h-SLG through in situ Raman measurements in an electrochemical cell as shown in schematic of **Figure 1**. We then recorded graphene-enhanced Raman spectra of different concentrations of MB on both p-SLG and h-SLG on the working electrode (WE) before assembling the electrochemical cell. Finally, we demonstrated the tunability of GERS enhancement by changing the chemical potential of the graphene while varying the applied potential.

2.1. In Situ Raman Spectroelectrochemical Analysis of p-SLG and h-SLG

Figure 2 shows the in situ spectroelectrochemical and voltammetric measurements of pristine and hydrogenated graphene. The Raman spectra recorded on p-SLG and h-SLG at various potentials during the cyclic voltammetry (CV) scan at a voltage sweep rate of 5 mV s^{-1} are shown in Figures 2a and 2b, respectively. The variation of the Raman G peak position (ω_G) for p-SLG and h-SLG as a function of electrode potential is depicted in Figure 2c. The G peak of p-SLG was observed to have a minimum value of ≈1583 cm^{-1} at the electrode potential of ≈0 V (vs Ag/AgCl), which corresponds to the charge neutrality point (CNP) of graphene.

Furthermore, the G peak of p-SLG blue-shifted upon the application of both positive and negative potentials (Figure 2a,c), which is consistent with our previous observations.[41] Quantitatively, the G peak shifted to 1592 and 1591 cm^{-1} (i.e., $\Delta\omega_G = 9$ and 8 cm^{-1}, respectively, relative to CNP) when the applied electrode potential is varied from +0.4 to −0.5 V (vs Ag/AgCl), respectively. With an applied electrochemical potential, the change in the G mode frequency is related to the C—C bond strength and the renormalization of the phonon energy.[41] Doping in graphene results in chemical bonding energy variation, thereby modifying the bond length and phonon frequencies, which leads to further changes in the G peak position.

Moreover, at the CNP, the phonon-generated electron–hole pairs cause the broadening of the G mode. In charged graphene, the Fermi level shifts away from the Dirac point and hence the generation of electron–hole pairs by phonons is suppressed, sharpening the G mode linewidth. This effect also results in a monotonous enhancement of the G peak intensity (height) within the measured potential window, consistent with previous reports.[41,42] The intensity variations of the G and 2D peaks and their ratio (i.e., I_{2D}/I_G) with potential are shown in Figure S1, Supporting Information. As higher potentials (both positive and negative) are applied on p-SLG, the intensity of the 2D peak decreases (Figure S1b, Supporting Information), in contrast with the variation of the G band intensity. Due to an increased number of charge carriers in doped graphene, the electron–phonon scattering dominates and decreases the intensity of the 2D peak.[30] Hence, the ratio I_{2D}/I_G changes significantly with the doping level of the graphene layer.

It was also observed that the shift in the 2D peak position for a positive applied potential is stronger than for a negative potential (Figure S1d, Supporting Information). This change is related

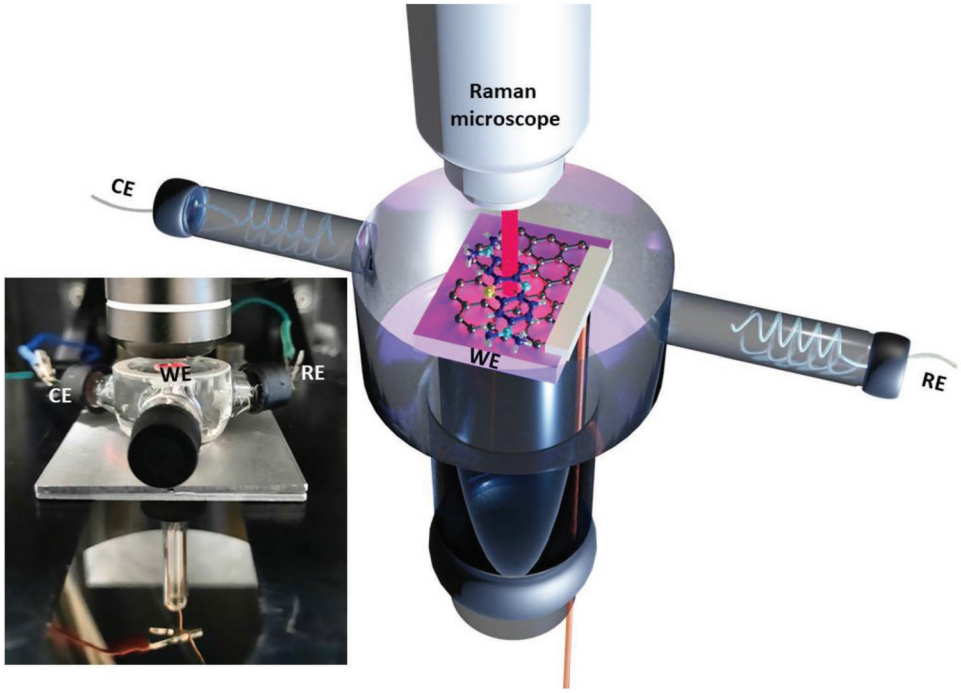

Figure 1. Schematic of the graphene-enhanced spectroelectrochemical sensor under the measurement conditions. The bottom-left inset is a photograph is of the device and was taken during in situ spectroelectrochemical measurements under 633 nm laser excitation.

to the C—C bond strength, as discussed previously.[41] Furthermore, the measurements were conducted for consecutive forward and reverse cycles, and the CNP of graphene was observed to be –0.2 V in the reverse cycle, which indicates

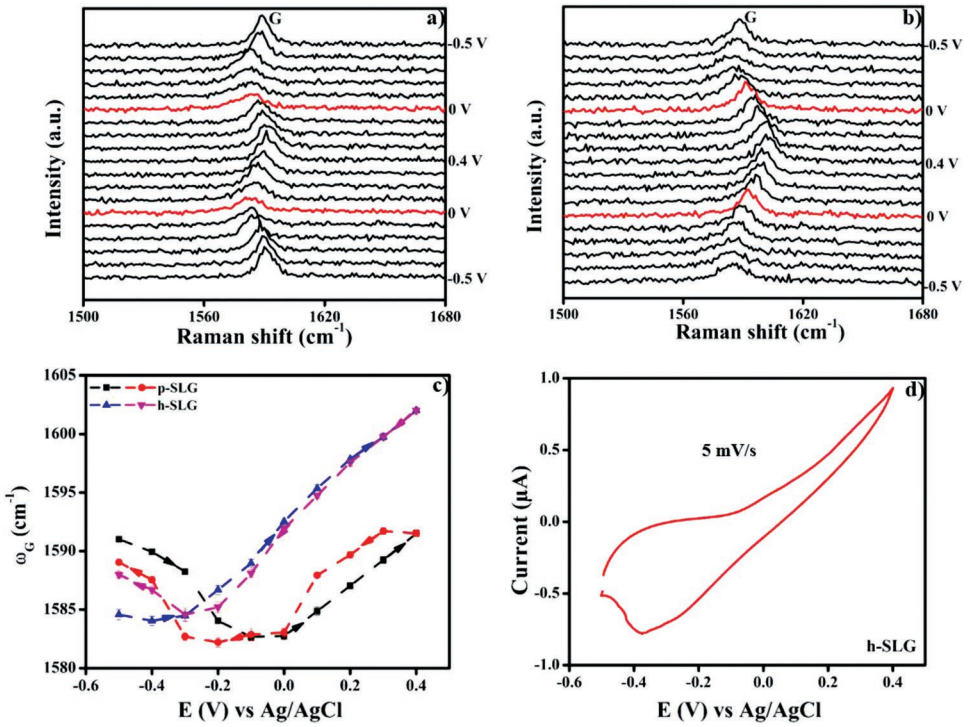

Figure 2. a,b) In situ Raman spectra showing the G peak position under the potential range –0.5 V to 0.4 V for forward and reverse cycles of electrochemical measurements, corresponding to p-SLG and h-SLG, respectively, c) comparison of G peak position shifts with respect to the applied potential for p-SLG and h-SLG samples here, the black, blue lines indicate forward cycle for p-SLG and h-SLG, respectively and red, violet lines indicate reverse cycles for p-SLG and h-SLG, respectively, and d) cyclic voltammogram of h-SLG at a scan rate of 5 mV s^{-1}. (Sample size, $n_{p\text{-}SLG}$ is 5.9 mm × 4.2 mm and $n_{h\text{-}SLG}$ is 5.02 mm × 3.4 mm).

slight irreversibility in the system (Figure 2c). The electrochemical behavior of p-SLG was investigated through CV at different scan rates, as shown in Figure S1e, Supporting Information. The 'rectangular' shapes of the voltammograms indicated dominant capacitive behavior due to charge transfer between the electrolyte and the electrode.

The partially hydrogenated graphene was prepared using our previously established protocol.[43] The detection of the presence of hydrogen on graphene (single and/or few-layer) has been a challenging task. To address this issue, we recently have demonstrated a chemical route to probe hydrogen in partially hydrogenated graphene with the assistance of the surface-enhanced Raman spectra technique,[43] where the probe hydrogen atoms were chemically replaced with a target functional group, and the Raman signal corresponding to that group has been studied. As the hydrogenated graphene used in this study has been prepared utilizing the same protocol, we expect a similar degree of functionalization of the graphene layer. The signature of partial hydrogenation is also clear from obtained weak Raman D mode intensity, as shown in Figure S2, Supporting Information. To probe the coverage of hydrogen on the graphene layer, we performed Raman map of the hydrogenated graphene. The nearly uniform distribution of the weak Raman D mode shoulder peak resembles the distribution of hydrogen on graphene. We also probed the stability of the hydrogene on partially hydrogenated graphene by recording the Raman signal of the sample while keeping it in ambient conditions for 90 days. A slight decrease in the Raman D mode is observed, as shown in Figure S2f,g, Supporting Information, which resemble a gradual release of hydrogen from graphene.

The in situ spectroelectrochemical data of h-SLG (Figure 2b,c) shows distinct differences from p-SLG (Figure 2a,c). For the h-SLG sample, the CNP of graphene was shifted to ≈–0.4 V, which corresponds to a ≈0.4 V shift relative to the p-SLG. It has been reported that pure h-SLG exhibited an electron-doped nature.[44] However, this shifting of the CNP toward a more negative potential can be attributed to hole doping from adsorbate molecules (primarily moisture) on the surface of h-SLG during the graphene transfer and electrode design.[25,44] Consequently, in thermal equilibrium, the work function of h-SLG is lower than that of p-SLG (≈4.6 eV of p-SLG/SiO_2/Si).[44]

Additionally, a monotonous enhancement of the G peak position was observed while the applied bias was tuned from –0.5 V to 0.4 V (Figure 2c, blue curve). Due to the limited potential window, the p-doped side of the bias dependence is inaccessible up to –0.5 V. The shift in the G peak position at the same applied electrochemical potential is higher in h-SLG than p-SLG. The G peak of h-SLG shifts to 1602 cm^{-1} (i.e., $\Delta\omega_G$ = 12 cm^{-1}, with respect to the CNP) upon application of 0.4 V (vs Ag/AgCl). An increase in the G peak intensity was observed while accessing higher potentials across the CNP, and it saturated after reaching ≈0 V (Figure S3a, Supporting Information). A monotonic decrease in the intensity of the 2D peak was observed in Figure S3b, Supporting Information, while the potentials increased and decreased with respect to the CNP (≈–0.4 V).

The variation of I_{2D}/I_G with applied potential shows a maximum at the CNP. It decreases for both higher and lower potentials, as shown in Figure S3c, Supporting Information, which can be interpreted as the effect of doping and electron–phonon scattering in the graphene layer, as discussed above. The frequency shift of the 2D band of hydrogenated graphene in Figure S3d, Supporting Information was also dependent on the doping. An increase in frequency was observed with applied electrochemical potential for electron and hole doping. As the h-SLG is naturally hole-doped, a higher shift in the 2D peak position (to 2657 cm^{-1}) was observed with respect to the CNP (2650 cm^{-1}) at higher potentials. Hence, $\Delta\omega_{2D}$ was 7 cm^{-1} when the highest accessible positive electrode potential of 0.4 V (vs Ag/AgCl) was applied. Furthermore, the CV of h-SLG at a scan rate of 5 mV s^{-1} is shown in Figure 2d. The absence of any redox peak in the CV indicates that there was no detectable amount of the probe molecule present. A CV corresponding to hydrogenated graphene at different scan rates is shown in Figure S3e, Supporting Information. To obtain better insight into doping, we performed a correlation analysis of the G and 2D Raman graphene bands (Figure S4, Supporting Information) that clearly shows the evolution of doping of individual samples upon external potential. The doping levels of pristine and hydrogenated graphene were calculated after disentangling the effect of strain and doping on the Raman shift of the G band.[45] Absolute doping levels were estimated by referring to the Fermi energy of graphene at ≈–4.6 eV.[42]

2.2. GERS-Based Sensing of Methylene Blue on p-SLG and h-SLG

In order to probe the MB molecules through the GERS effect, 10^{-6} M of MB was deposited on p-SLG, h-SLG, and SiO_2/Si. The obtained Raman spectra of the samples are shown in **Figure 3**a. The molecules deposited on the p-SLG and h-SLG show intense Raman features (red and blue spectra, respectively). The Raman modes with frequencies centered around 1395, 1498, and 1622 cm^{-1} are assigned to C—N symmetric stretching, asymmetrical stretching of C—C, and C—C ring stretching of MB, respectively, and are shown in the inset of Figure 3a.[28,36] The graphene Raman peaks (i.e., G and 2D) are also visible. Furthermore, the absence of the graphene D band in MB/p-SLG indicates no covalent bond existed between the SLG and MB.[40]

However, the electrostatic interaction of the MB molecules with the graphene affects their electrochemical activity. No pronounced signal corresponding to the Raman modes of the probe molecules was observed (Figure 3a, black curve) for the MB molecules deposited on the SiO_2/Si substrate (MB/SiO_2/Si) following the same procedure as MB/p-SLG and MB/h-SLG. We relate the absence of Raman modes of MB on SiO_2/Si as follows: the fluorescence from molecules on SiO_2/Si substrate results in a background emission which eventually suppresses the Raman modes.[13] On the contrary, on graphene, fluorescence is quenched, and Raman modes are enhanced due to the GERS effect. Moreover, the studied concentrations of the molecule were very low. After coating the molecules, we soaked the substrate in water for cleaning the overgrown MB molecules from the device, which further reduced the number of molecules on all of the substrates including SiO_2/Si. This lack of signal indicates that the Raman signal of MB on both types of graphene is strongly amplified due to the GERS effect. Note that the energy difference

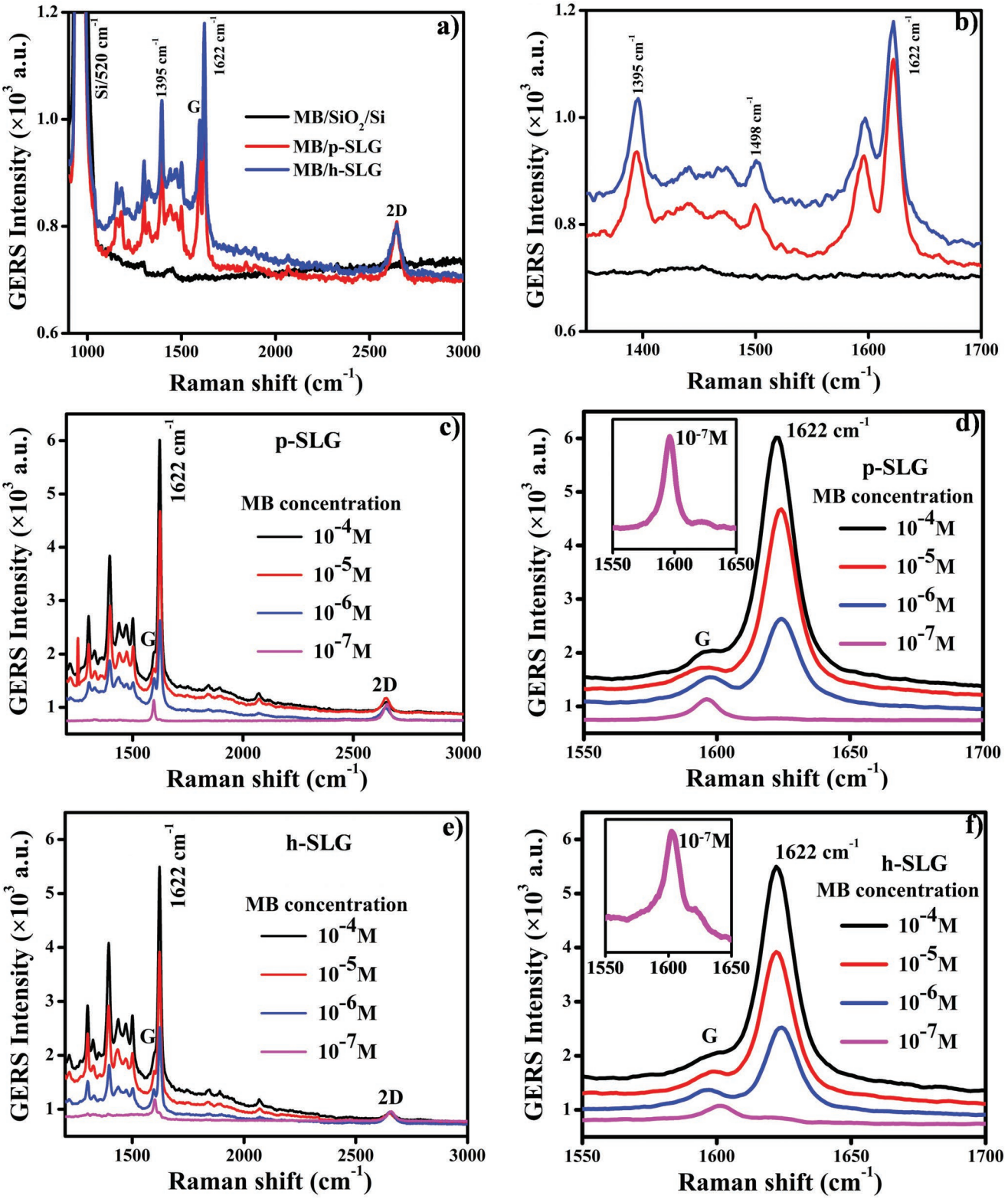

Figure 3. a) GERS signal of MB molecules with a concentration of 10^{-7} M on SiO_2/Si (black), p-SLG (red), and h-SLG (blue) substrates with 633 nm laser, b) zoomed spectra corresponding to a of MB peaks around 1622 cm^{-1} along with the G mode of graphene. Almost no intensity corresponding to MB was observed on the SiO_2/Si substrate. c,d) GERS spectra of MB adsorbed on p-SLG and zoomed spectra corresponding to a of MB peaks around 1622 cm^{-1}. d,f) GERS spectra of MB adsorbed on h-SLG and zoomed spectra corresponding to a of MB peaks around 1622 cm^{-1}. The pink spectra in the inset of (d) and (f) are the spectra of MB around 1622 cm^{-1} for 10^{-7} M of MB on p- and h-SLG.

between the HOMO and LUMO energy states of MB is nearly resonant with the excitation laser energy, that is, $\hbar\omega_0 = E_L - E_H$, where ω_0 is the laser frequency, and E_L and E_H are the LUMO and HOMO energy levels. It satisfies the necessary resonant condition for obtaining GERS.

Furthermore, Raman enhancement is also related to the resonance between the Fermi energy of the graphene, the HOMO/LUMO energy levels of the molecules, and the energy of the incident laser beam.[46] The molecular structural symmetry of probe molecules and graphene also play an important role.[18,47] The similar hexagonal carbon ring structures of the MB molecule and the graphene enable efficient charge transfer, thus enhancing the Raman signal.[48]

Due to GERS, even a low concentration of MB can be detected, which was not possible when SiO_2/Si was used as the substrate. The topography of pristine graphene covered with MB molecules (10^{-6} M) was further characterized using atomic force microscopy (AFM) (Figure S5a,b, Supporting Information). However, due to extremally low number of the molecules on the substrate no significant differences in the height profile for these two samples were observed, as seen in Figure S4c, Supporting Information.

To estimate the LOD for MB molecules, the GERS spectra were also measured for different concentrations of MB (10^{-7} to 10^{-4} M), on p- and h- SLG, as shown in Figure 3c–f. A systematic variation of the strong GERS signals of MB was detected up to 10^{-6} M. However, on p-SLG, the signal lowered significantly at 10^{-7} M, as evident in Figure 3c,d (inset of Figure 3d). In contrast, for h-SLG, the Raman peak corresponding to MB remains more pronounced than on p-SLG (pink spectrum in Figure 3d,e, inset of Figure 3f) at 10^{-7} M. Hence, the LOD for h-SLG is lower (<10^{-7} M) than that of p-SLG (≈10^{-7} M). LOD of the molecules depends on the method of molecule deposition as rinsing process followed by soaking removes any excess molecules. To date, not many works have been reported of MB sensing on graphene substrates. The obtained LOD in our work is one of the best among the previously published reports. We have included a comparison table, Table S1, Supporting Information, indicating the LOD of the previously reported works.[13,39,49]

Based on the doping levels obtained from the correlation analysis, the mechanism of the GERS effect on p- and h-SLG can be understood through the band diagram (**Figure 4**). Note that the obtained Raman spectra (Figure S6, Supporting Information) of graphene after coating the molecules show slight doping in graphene caused by charge transfer at the interface, which makes the relative shift of the HOMO (–5.67 eV) and LUMO (–3.81 eV) levels of MB.[50] However, we will use the reported values to establish the mechanism of the observed GERS effect. The Fermi energy of p-SLG is found to be shifted by ≈–0.17 eV from the CNP (≈–4.6 eV) and lies nearly at the middle of the gap between the HOMO and LUMO energy levels of molecular MB as shown in Figure 4a. Thus, the GERS effect is attributed to the fulfilment of $\hbar\omega_0 = E_L - E_H$ condition. Upon hydrogenation, the graphene becomes increasingly p-doped. The Fermi energy is shifted by ≈–0.30 eV (from CNP) and approaches nearer to the HOMO energy level of MB, which brings the system nearer to an additional energy resonant condition ($E_F = E_H + \hbar\omega_q$). Thus, h-SLG tend to show slightly stronger GERS signals compared with p-SLG (Figures 3b and 4b).[13,16,18,51,52]

2.3. GE-SPECS for Sensing of MB on p-SLG and h-SLG

The graphene-enhanced Raman signal was also used to investigate spectroelectrochemical sensing of MB molecules under 0.8 mW 633 nm laser excitation as a function of applied electrochemical potential. Cyclic voltammetry measurements show similar sensing behavior as observed in GERS sensing. A comparison of CVs corresponding to p-SLG and h-SLG covered with molecules of different concentrations is shown in Figure S7a–f, Supporting Information. The lowest concentration of MB molecules for p-SLG that can be detected electrochemically was found to be >10^{-7} M, as shown in Figure S7a, Supporting Information. However, in h-SLG, it was found to be <10^{-7} M, as a small redox peak was observed around 0.15 V even at 10^{-7} M, as shown in Figure S7b, Supporting Information. More pronounced redox peaks were observed in both p- and h-SLG for the higher concentrations of MB, as shown in Figure S7c–f, Supporting Information. For in situ spectroelectrochemical measurements, we used concentrations of 10^{-6} M, which showed systematic variations in the intensity of the MB Raman

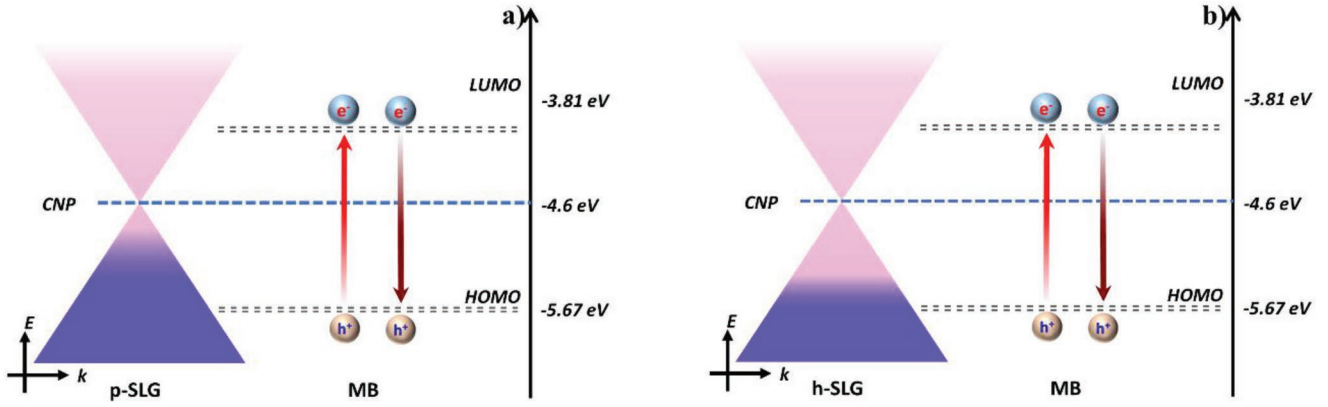

Figure 4. Energy band diagrams corresponding to a) p-SLG and b) h-SLG showing efficient charge transfer between h-SLG and MB (compared with the charge transfer between p-SLG and MB) as the Fermi energy of h-SLG is nearly resonant with the HOMO of MB.

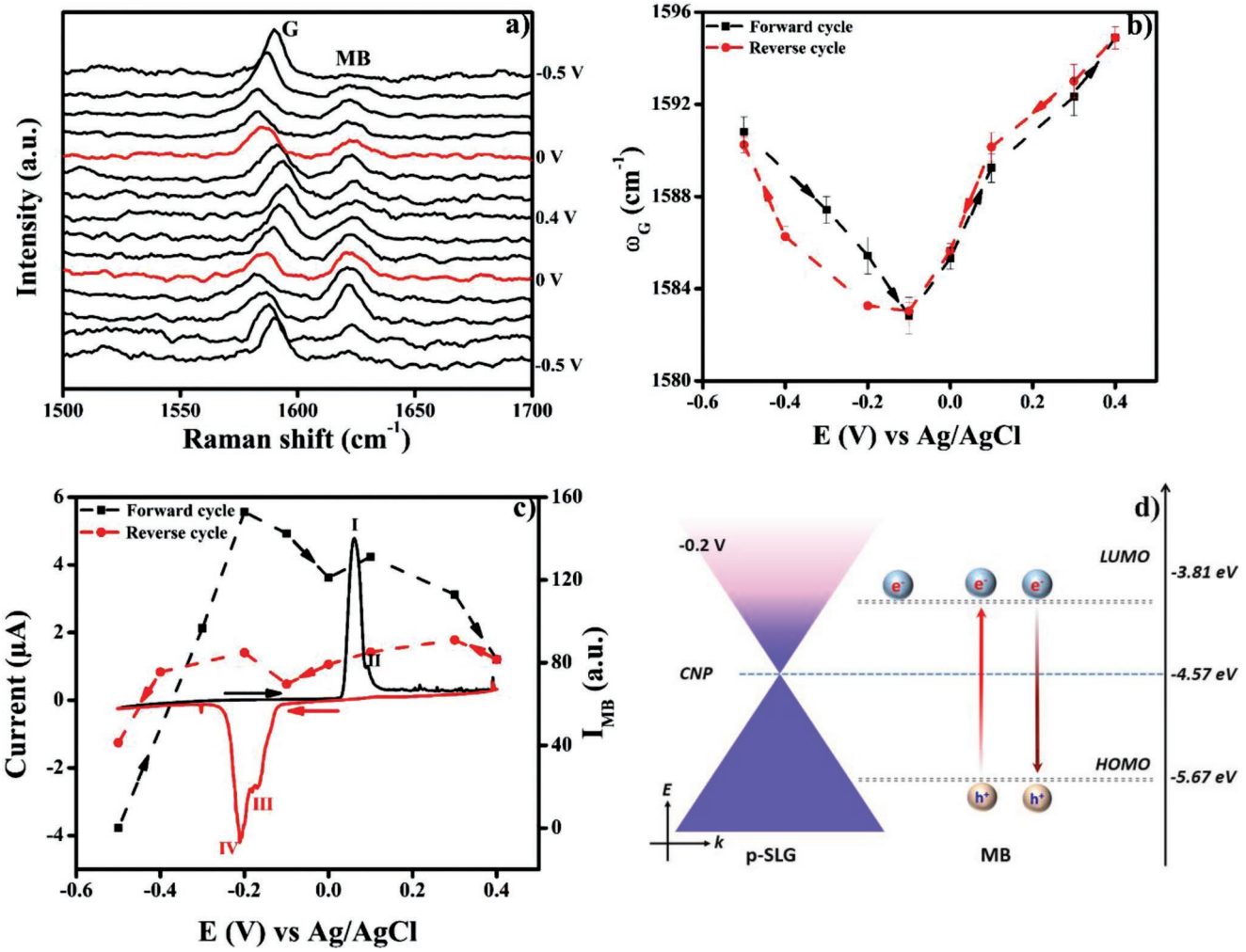

Figure 5. a) In situ Raman spectra at different potentials (swept from –0.5 V to +0.4 V, and +0.4 V to–0.5 V), b) G peak shift versus applied potential, c) CVs at a scan rate of 5 mVs^{-1} combined with MB peak (1622 cm^{-1}) intensity at different applied potentials (continuous line represents the CV sweep with redox peaks, arrows indicate the direction of potential sweep in CV, dotted lines show the MB peak intensity at different potentials) and d) band diagram showing the possible charge transfer mechanism between the Fermi energy of graphene and the HOMO at –5.67 V of MB for p-SLG (Fermi energy of pristine graphene shifted by the application of –0.2 V). The figure is drawn based on the data obtained from the Raman correlation plot shown in Figure S4c, Supporting Information and ref. [42] (Sample size, $n_{MB/p\text{-}SLG}$ is 5.03 mm × 3.48 mm).

peak with the application of potentials, as shown in **Figure 5**a. Although the spectra obtained from MB/p-SLG showed intense Raman vibration modes of MB, as discussed in the previous section and shown in Figure 3, in the presence of an aqueous electrolyte, without applying any electrode potential, the relative intensity of this characteristic feature decreased, and a fluorescence background was observed (Figure S8, Supporting Information), which is a common occurrence in such experimental design.

Figure 5a shows the Raman spectra of the MB/p-SLG composite recorded in situ during the CV scan at the sweep rate of 5 mV s^{-1}. The corresponding shift of the G mode is shown in Figure 5b. The variation of the intensity of the 1622 cm^{-1} MB Raman mode obtained from Figure 5a is shown in Figure 5c together with the CV. Unlike G mode of graphene, the Raman modes of MB molecule does not resemble significant phonon energy softening with the applied potential.[48] Hence, the G mode of graphene and Raman modes of MB show different trends in Raman measurement with applied electrochemical potential. The evaluation of the G mode position in MB/p-SLG is similar to the mode of pure p-SLG, as discussed in the previous section. However, the shift of the CNP toward a more negative potential is due to MB-induced *p*-doping in p-SLG. This observation also supports the charge transfer mechanism shown in Figure 4a. The variations of intensities of G and 2D peaks for the MB/p-SLG sample at various electrode potentials are also shown in Figure S9a,b, Supporting Information and have a similar trend to p-SLG, as discussed above.

In order to understand the effect of electrochemical charging on the resulting GERS spectra, we need to consider three different processes in the system, that is, i) electrochemical activity of MB, ii) position of Fermi energy of graphene, and iii) photo-electrochemical stability of MB on the graphene substrate. First, the voltammogram of MB on p-SLG in Figure 5c

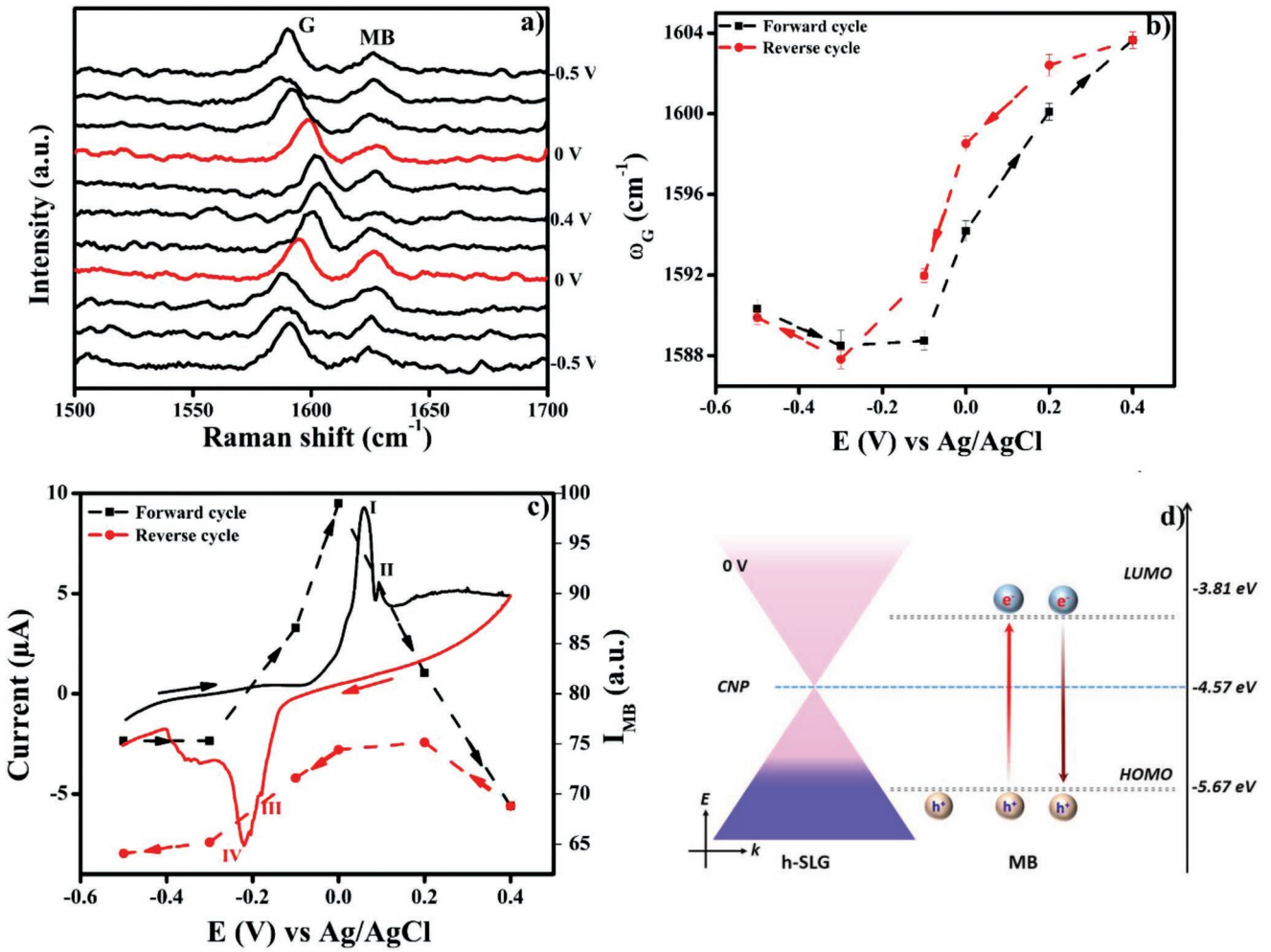

Figure 6. a) In situ Raman spectra at varying potentials (swept from –0.5 V to +0.4 V, and +0.4 V to–0.5 V), b) G peak position variation with applied potential, c) Variation of MB peak intensity with potential and corresponding CVs for a 5 mV s^{-1} scan rate potentials (continuous line represents the CV sweep with redox peaks, arrows indicate the direction of potential sweep in CV, dotted lines show the MB peak intensity at different potentials) and d) Band diagram showing the possible charge transfer mechanism between the Fermi energy of graphene and the HOMO at –5.67 V of MB for h-SLG (Fermi energy of hydrogenated graphene is shifted as a result of hole doping). The Figure is drawn based on the data obtained from the Raman correlation plot shown in Figure S4d, Supporting Information and ref. [42] (Sample size, $n_{MB/h\text{-}SLG}$ is 4.2 mm × 3.56 mm).

shows the anodic peaks I and II that appeared at 0.06 and 0.09 V, respectively, whereas cathodic peaks III and IV appear at –0.17 and –0.20 V, respectively. As the CV scan was initiated at –0.5 V, reduced-state leucomethylene blue (LMB) was obtained as the very first stage. Intermediate-state HMB• and oxidized-state MB were obtained with the gradual change of the potential toward +0.4 V. Hence, the first anodic peak (I) is related to the oxidation or phase transition of LMB to HMB•, and the second anodic peak (II) is related to the further oxidation of HMB• to MB. The cathodic peaks correspond with the reduction of MB to HMB• (III) and the further reduction of the radical cation HMB• to LMB (IV).[48,53–55] These dual peaks appear due to a one-electron transfer during the phase transition MB ↔ HMB• and two-electron transfer for the transition MB ↔ LMB for the cathodic and anodic scans.[48] Farsi et al. have observed one reduction and two oxidation peaks of MB on a nanostructured metal oxide semiconductor surface,[31] where MB in solution was reduced by two sequential one-electron transfer processes for faster conversion of the intermediate-state semi-MB to LMB, then to MB. However, MB immobilized on surfaces through electrostatic interactions showed a different electrochemical behavior.[56] Additionally, the potential of the MB absorbed on different substrates also depends on the pH of the electrolyte and the substrate used.[53–55,57,58] Furthermore, the appearance of two sequential reduced and corresponding oxidized states of MB was also observed in the CVs for all the scan rates (Figure S7c, Supporting Information).

As shown in Figure 5c, while the potential swept from –0.5 to +0.4 V, the Raman intensity of MB increased from –0.5 V to reach its maximum at –0.2 V. Then it decreases and goes to a minimum at –0.5 V during the reverse cycle. The minimum Raman intensity at –0.5 V is due to the fact that the LMB state shows absorption maxima in the ultraviolet range. Thus, the molecules remain undetectable under 633 nm laser excitation.[54] The increased intensity at –0.2 V is due to the oxidation of the LMB molecule to the HMB• and MB states.[54] As MB

showed an absorption maxima around 610 and 662 nm, it fulfils the $\hbar\omega_0 = E_L - E_H$ criterion, showing a strong enhancement of Raman signals.

Second, note that the CV and the Raman of intensity peaks do not correspond to the same potential. This can be understood as the energy resonance effect. The Fermi energy of graphene takes its highest value at the minimum applied potential, –0.5 V. With increasing applied potential, the Fermi energy decreased. Simultaneously, the LMB was oxidized to HMB$^{\bullet}$ and MB, causing a gradual enhancement of the resonance charge transfer between graphene and the LUMO level of the MB molecule. As a result, the Raman intensity increased up to the applied potential of –0.2 V. However, at the higher applied potential, > –0.2 V, the Fermi energy of graphene gradually starts to lose resonance with the LUMO energy state of MB, and the Raman intensity gradually decreases. The GERS process for MB and HMB$^{\bullet}$ states at the applied potential of –0.2 V is schematically shown in Figure 5d.

Third, the lower Raman intensity at the reverse cycle can be correlated to the photo-electrochemical stability of MB on the graphene substrate. In this case, lowering the intensity could be due to the gradual release of MB molecules from graphene to the solution and the eventual electrochemical degradation of MB under the laser excitation.

In the case of the h-SLG substrate covered with MB molecules, the nature of the doping was similar to the pristine h-SLG sample, as estimated from the G band shift with an applied potential (Figures 2 and **6**a). The $\Delta\omega_G$ estimated here were 15 and 2 cm^{-1}, relative to CNP for 0.4 and –0.5 V (vs Ag/AgCl), respectively (Figure 6b). Hole doping leads the CNP shift to a negative potential, and a lower shift in G peak position is seen at the negative potential.

The intensity variation of the MB peak (1622 cm^{-1}) with applied electrochemical potential and the corresponding voltammogram are shown in Figure 6c. Measurements were started at the most negative potential of –0.5 V. With increasing electrochemical potential, the intensity of the MB peak increased and reached a maximum at ≈0 V. Further increasing the potential led to a decrease in the Raman intensity. The observation can be rationalized based on the three effects similarly as discussed above together with the change in conductivity of h-SLG with respect to SLG. It is evident that in contrast with the p-SLG, h-SLG shows significant Raman intensity at –0.5 V. Due to hydrogenation, graphene becomes more resistive, and a fraction of molecules on h-SLG may remain electrochemically inactive. Thus, those molecules remained at MB state at the applied potential of –0.5 V, may still contribute to the Raman intensity. This is also consistent with the observed lower magnitude of current peaks in CV. Now, Figure S10, Supporting Information reveals that h-SLG is more p-type in nature than the p-SLG, resulting in a lower Fermi energy with the same applied bias. Thus, the Fermi energy of h-SLG remained between the HOMO and LUMO levels even at the minimum applied potential (–0.5 V). As the potential increased, a gradual enhancement to the Raman intensity of MB was observed. This is due to the conversion from LMB to MB states. At ≈0 V applied bias, the near resonance energy to the HOMO level of the MB cause efficient energy transfer resulting strong Raman signal.[13,16,18,51,52] The position of the Fermi energy of h-SLG at ≈0 V and the HOMO-LUMO energy of MB is schematically shown in Figure 6d. However, the overall Raman intensity starts reducing after 0 V. It continues in a reduced-intensity state during the reverse cycle, which is attributed to the continuous exposure of the sample to the laser, causing mild degradation.

The CM enhancement (GERS) is associated with the filling of the laser energy with the gap between HOMO – LUMO of the molecule, that is, $\hbar\omega_0 = E_L - E_H$, and the position of the Fermi energy of graphene with respect to the HOMO/LUMO of the molecule. The Fermi energy position determines the charge transfer efficiency, as observed in Figures 5 and 6 for pristine and hydrogenated graphene, respectively. However, with the applied potential, oxidation states of the probe MB molecule change, which restricts us to probe the resonance match between HOMO/LUMO and the Fermi energy of graphene that was theoretically shown to have the highest GERS effect.[16] Theoretically the influence of those effects are similar.[16] However, tuning laser energy in such small range is a big challenge. Additionally, a tunable energy laser source is rare. Furthermore, we performed the GERS measurement utilizing different discrete laser excitations of energies 1.96, 2.33, and 2.41 eV (Figure S11, Supporting Information), where 1.96 eV is the resonance laser energy. We observed that the GERS enhancement is negligible while the excitation energy is off-resonant. It is stressed that this study aims to electrochemically amplify the laser resonance enhancement with the application of external bias.

2.4. Specificity of the GE-SPECS on p-SLG and h-SLG

We have performed sensing of another organic molecule Nile blue (NB), separately. The 1.96 eV laser of power 0.8 mW was used to obtain the Raman signals of NB molecules. The Raman spectra corresponding to different substrates are shown in **Figure 7**. Interestingly, the limit of detection for NB was found to be 10^{-7} M on p- and h-SLG on SiO_2/Si. As NB resembles a completely different Raman feature, the molecules can be identified up to a concentration of 10^{-7} M. Thus, the designed GE-SPECS is robust and not specific to just one particular molecule.

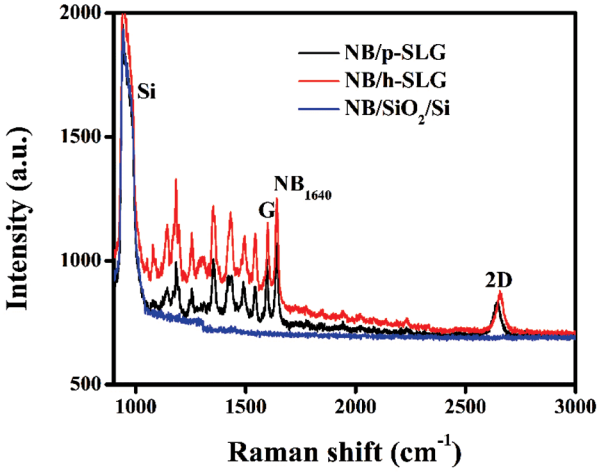

Figure 7. Raman spectra of NB molecules (10^{-7} M) on SiO_2/Si (blue), p-SLG (black), and h-SLG (red).

3. Conclusion

We have demonstrated efficient novel spectroelectrochemical sensors based on graphene, GE-SPECSs. Based on the chemical enhancement process, GERS is selective to specific molecules that fulfil the resonance conditions. However, we utilized the tunable work function of graphene to circumvent the rigid energy-specific nature of GERS enhancement. We found that the sensitivity of the sensors can be tuned by both covalent and electrostatic doping in the graphene layer. The highly p-doped h-SLG shows a LOD superior to that of p-SLG, where the LOD for p- and h-SLG were found to be $<10^{-6}$ and $<10^{-7}$ M, respectively, comparable to standard metal nanoparticle-based surface-enhanced SPECSs. We have demonstrated that the GERS effect can be greatly enhanced by tuning the Fermi energy of graphene by applying an external potential. Additionally, it enabled us to probe different oxidation states of a probe molecule, MB. Graphene is an environmentally friendly, highly stable, and cheap material. Thus, our graphene-based aqueous electrochemical sensors have tremendous advantages for potential practical utilization in biomedical applications.

4. Experimental Section

Material Synthesis: As reported previously, SLG was grown via the standard CVD method.[19] In brief, a copper foil was annealed at 1000 °C for 30 min under a 50 sccm hydrogen flow. Subsequently, CH_4 (1 sccm) was introduced into the chamber for 20 min. Finally, the system was cooled under the same flow of H_2. The as-grown graphene was transferred on a SiO_2/Si substrate by the wet transfer method using nitrocellulose as the carrier polymer. Partially hydrogenated graphene samples were prepared in a high-pressure autoclave as described in an earlier study.[19] The autoclave was flushed several times with hydrogen to remove the air. Then, the autoclave was filled with hydrogen at a pressure of 5 bar. Finally, the temperature was increased to 200 °C. The hydrogenation process was carried out for 2 h at a pressure of ≈8 bar. After that, the hydrogen was flushed out from the autoclave, and the samples were removed while the system was cooled to room temperature.

Methylene blue in its powder form was purchased from Sigma Aldrich and its solution was prepared in de-ionized water. Initially, the highest concentration of molecules was prepared and lower concentrations were prepared by diluting as shown in Figure S12, Supporting Information. MB molecules were deposited onto graphene using the soaking method, where SiO_2/Si substrate was soaked in an aqueous solution of MB of various concentrations for 2 min, followed by rinsing in water for 30 min and drying with argon flow.

In Situ Spectroelectrochemical Measurements: In situ Raman spectroelectrochemistry measurements were performed in a custom-made three-electrode quartz electrochemical cell during CV study. The complete spectroelectrochemical cell in the measurement condition is schematically shown in Figure 1, where the bottom-left inset is a real picture of the experimental setup. For the device, pristine and hydrogenated graphene on SiO_2/Si substrates were used as the WE, platinum wire as the counter electrode (CE), and chlorinated Ag wire as the reference electrode (RE). The WE was connected with copper wire, and Ag paste was used to create a solid connection with the graphene. Finally, we used Torr Seal epoxy resin to cover the Ag paste and the exposed Cu wire to avoid unwanted reactions. The as-prepared samples were left to dry for 24 h and later assembled in the electrochemical cell for measurements. A 0.1 M KCl (Sigma Aldrich) aqueous solution was used as the electrolyte, and the CV measurements were performed in the potential range −0.5 to +0.4 V (vs Ag/AgCl). Picture of the as-designed WE before assembling the cell is shown in Figure S12, Supporting Information.

Electrochemical measurements were performed with a potentiostat (Autolab PGSTAT 30, Metrohm) equipped with a low-current module working at a current range with a lower limit of 10 pA. The Raman spectra were recorded during the CV measurements using a LabRAM HR spectrometer (Horiba Jobin Yvon) interfaced to an Olympus BX-41 microscope and equipped with a 633 nm HeNe laser of excitation power ≈0.8 mW. All the spectra were acquired with a grating having a groove density of 600 lines mm^{-1} and a long working distance 100× objective. All the Raman peaks were fitted using pseudo-Voigt function.

AFM Measurements: The topographic analysis was performed using AFM Dimension Icon (Bruker). Images were obtained in peak force mode using standard Bruker ScanAsyst-Air AFM cantilevers.

Statistical Analysis: 1) Pre-processing of data: all the data analysis was performed using OriginPro 8.5 software. The Raman spectra shown in figures are plotted from raw data with baseline correction done using baseline correction tool of Origin. 2) Data presentation: peak fitting was done using PeakFit version 4.2 software. The error bars in plots were used from the fitted data. Additionally, the correlation plots were performed using MATLAB. 3) Sample size: $n_{\text{p-SLG}}$ is 5.9 mm × 4.2 mm and $n_{\text{h-SLG}}$ is 5.02 mm × 3.4 mm, $n_{\text{MB/p-SLG}}$ is 5.03 mm × 3.48 mm and $n_{\text{MB/h-SLG}}$ is 4.2 mm × 3.56 mm.

4) Statistical methods: five devices were tested for all the sample types and systematic behavior were observed. 5) Software used for statistical analysis: OriginPro 8.5, PeakFit, MATLAB.

Supporting Information

Supporting Information is available from the Wiley Online Library or from the author.

Acknowledgements

The work was supported by project No. LTAUSA19001 by the Ministry of Education, Youth and Sports of the Czech Republic.

Conflict of Interest

The authors declare no conflict of interest.

Data Availability Statement

The data that support the findings of this study are available from the corresponding author upon reasonable request.

Keywords

charge transfer, graphene-enhanced Raman spectroscopy, in situ spectroelectrochemistry, methylene blue, spectroelectrochemical sensors

Received: March 3, 2022
Revised: April 8, 2022
Published online: June 7, 2022

[1] M. Fleischmann, P. J. Hendra, A. J. McQuillan, *Chem. Phys. Lett.* **1974**, *26*, 163.
[2] X. H. Vu, N. D. Dien, T. T. Ha Pham, T. T. Trang, N. X. Ca, P. T. Tho, N. D. Vinh, P. Van Do, *RSC Adv.* **2020**, *10*, 38974.
[3] A. Campion, C. Harris, *Chem. Soc. Rev.* **1998**, *27*, 241.
[4] X. Ling, L. Xie, Y. Fang, H. Xu, H. Zhang, J. Kong, M. S. Dresselhaus, J. Zhang, Z. Liu, *Nano Lett.* **2010**, *10*, 553.

[5] X. Ling, J. Zhang, *J. Phys. Chem. C* **2011**, *115*, 2835.
[6] N. Jung, A. C. Crowther, N. Kim, P. Kim, L. Brus, *ACS Nano* **2010**, *4*, 7005.
[7] G. Bharath, R. Madhu, S. M. Chen, V. Veeramani, D. Mangalaraj, N. Ponpandian, *J. Mater. Chem. A* **2015**, *3*, 15529.
[8] G. Bharath, R. Madhu, S. M. Chen, V. Veeramani, A. Balamurugan, D. Mangalaraj, C. Viswanathan, N. Ponpandian, *J. Mater. Chem. B* **2015**, *3*, 1360.
[9] G. Bharath, V. Veeramani, S. M. Chen, R. Madhu, M. Manivel Raja, A. Balamurugan, D. Mangalaraj, C. Viswanathan, N. Ponpandian, *RSC Adv.* **2015**, *5*, 13392.
[10] X. Ling, L. G. Moura, M. A. Pimenta, J. Zhang, *J. Phys. Chem. C* **2012**, *116*, 25112.
[11] X. Ling, J. Zhang, *Small* **2010**, *6*, 2020.
[12] Y. Zhao, Y. Xie, Z. Bao, Y. H. Tsang, L. Xie, Y. Chai, *J. Phys. Chem. C* **2014**, *118*, 11827.
[13] S. Feng, M. Cristina dos Santos, B. R. Carvalho, R. Lv, Q. Li, K. Fujisawa, A. L. Elías, Y. Lei, N. Perea-López, M. Endo, M. Pan, M. A. Pimenta, M. Terrones, *Sci. Adv.* **2016**, *2*, 1600322.
[14] A. Silver, H. Kitadai, H. Liu, T. Granzier-Nakajima, M. Terrones, X. Ling, S. Huang, *Nanomaterials* **2019**, *9*, 516.
[15] H. Lai, F. Xu, Y. Zhang, L. Wang, *J. Mater. Chem. B* **2018**, *6*, 4008.
[16] E. B. Barros, M. S. Dresselhaus, *Phys. Rev. B – Condens. Matter Mater. Phys.* **2014**, *90*, 035443.
[17] X. Ling, J. Wu, W. Xu, J. Zhang, *Small* **2012**, *8*, 1365.
[18] S. Huang, X. Ling, L. Liang, Y. Song, W. Fang, J. Zhang, J. Kong, V. Meunier, M. S. Dresselhaus, *Nano Lett.* **2015**, *15*, 2892.
[19] V. Valeš, K. Drogowska-Horná, V. L. P. Guerra, M. Kalbáč, *Sci. Rep.* **2020**, *10*, 4516.
[20] Y. J. Yu, Y. Zhao, S. Ryu, L. E. Brus, K. S. Kim, P. Kim, *Nano Lett.* **2009**, *9*, 3430.
[21] H. Gao, L. Wang, J. Zhao, F. Ding, J. Lu, *J. Phys. Chem. C* **2011**, *115*, 3236.
[22] J. S. Burgess, B. R. Matis, J. T. Robinson, F. A. Bulat, F. K. Perkins, B. H. Houston, J. W. Baldwin, *Carbon N. Y.* **2011**, *49*, 4420.
[23] J. H. Jørgensen, A. G. Čabo, R. Balog, L. Kyhl, M. N. Groves, A. M. Cassidy, A. Bruix, M. Bianchi, M. Dendzik, M. A. Arman, L. Lammich, J. I. Pascual, J. Knudsen, B. Hammer, P. Hofmann, L. Hornekaer, *ACS Nano* **2016**, *10*, 10798.
[24] H. L. Poh, Z. Sofer, M. Pumera, *Electrochem. Commun.* **2012**, *25*, 58.
[25] L. Jiang, W. Fu, Y. Y. Birdja, M. T. M. Koper, G. F. Schneider, *Nat. Commun.* **2018**, *9*.
[26] E. Forgacs, T. Cserháti, G. Oros, *Environ. Int.* **2004**, *30*, 953.
[27] Z.-M. Xiong, X. Mao, M. Trappio, C. Arya, J. el Kordi, K. Cao, *Sci. Rep.* **2021**, *11*, 10871.
[28] R. R. Naujok, R. V. Duevel, R. M. Corn, *Langmuir* **1993**, *9*, 1771.
[29] A. Esokkiya, S. Sudalaimani, K. Sanjeev Kumar, P. Sampathkumar, C. Suresh, K. Giribabu, *ACS Omega* **2021**, *6*, 9528.
[30] D. M. Basko, S. Piscanec, A. C. Ferrari, *Phys. Rev. B* **2009**, *80*, 165413.
[31] H. Farsi, S. A. Hosseini, *J. Solid State Electrochem.* **2013**, *17*, 2079.
[32] J. Wang, F. Wang, S. Dong, *J. Electroanal. Chem.* **2009**, *626*, 1.
[33] D. B. Gorle, M. A. Kulandainathan, *RSC Adv.* **2016**, *6*, 19982.
[34] P. Yaiwong, N. Semakul, S. Bamrungsap, J. Jakmunee, K. Ounnunkad, *Bioelectrochemistry* **2021**, *142*, 107944.
[35] G. N. Xiao, S. Q. Man, *Chem. Phys. Lett.* **2007**, *447*, 305.
[36] R. V. William, G. M. Das, V. R. Dantham, R. Laha, *Sci. Rep.* **2019**, *9*, 10771.
[37] J. A. Anastasopoulos, A. Soto Beobide, A. C. Manikas, G. A. Voyiatzis, *J. Raman Spectrosc.* **2017**, *48*, 1762.
[38] P. Ren, W. Zhou, X. Ren, X. Zhang, B. Sun, Y. Chen, Q. Zheng, J. Li, W. Zhang, *Nanotechnology* **2020**, *31*, 1.
[39] Q. Hao, S. M. Morton, B. Wang, Y. Zhao, L. Jensen, T. Jun Huang, *Appl. Phys. Lett.* **2013**, *102*, 011102.
[40] N. S. Kaya, A. Yadav, M. Wehrhold, L. Zuccaro, K. Balasubramanian, *ACS Omega* **2018**, *3*, 7133.
[41] M. Kalbac, A. Reina-Cecco, H. Farhat, J. Kong, L. Kavan, M. S. Dresselhaus, *ACS Nano* **2010**, *4*, 6055.
[42] A. Das, S. Pisana, B. Chakraborty, S. Piscanec, S. K. Saha, U. V. Waghmare, K. S. Novoselov, H. R. Krishnamurthy, A. K. Geim, A. C. Ferrari, A. K. Sood, *Nat. Nanotechnol.* **2008**, *3*, 210.
[43] K. Drogowska, P. Kovaříček, M. Kalbáč, *Chem. – A Eur. J.* **2017**, *23*, 4073.
[44] B. R. Matis, J. S. Burgess, F. A. Bulat, A. L. Friedman, B. H. Houston, J. W. Baldwin, *ACS Nano* **2012**, *6*, 17.
[45] J. E. Lee, G. Ahn, J. Shim, Y. S. Lee, S. Ryu, *Nat. Commun.* **2012**, *3*, 1024.
[46] V. Valeš, P. Kovaříček, M. Fridrichová, X. Ji, X. Ling, J. Kong, M. S. Dresselhaus, M. Kalbáč, *2D Mater.* **2017**, *4*, 025087.
[47] S. Chattopadhyay, M. S. Li, P. Kumar Roy, C. T. Wu, *Analyst* **2015**, *140*, 3935.
[48] S. H. A. de Nicolai, P. R. P. Rodrigues, S. M. L. Agostinho, J. C. Rubim, *J. Electroanal. Chem.* **2002**, *527*, 103.
[49] Q. Hao, B. Wang, J. A. Bossard, B. Kiraly, Y. Zeng, I. K. Chiang, L. Jensen, D. H. Werner, T. J. Huang, *J. Phys. Chem. C* **2012**, *116*, 7249.
[50] H. Seema, K. Christian Kemp, V. Chandra, K. S. Kim, *Nanotechnology* **2012**, *23*, 355705.
[51] G. Haider, R. Ravindranath, T. P. Chen, P. Roy, P. K. Roy, S. Y. Cai, H. T. Chang, Y. F. Chen, *Nat. Commun.* **2017**, *8*, 256.
[52] R. S. Swathi, K. L. Sebastian, *J. Chem. Phys.* **2008**, *129*, 054703.
[53] T. Sagara, J. Iizuka, K. Niki, *Langmuir* **1992**, *8*, 1018.
[54] N. G. Tognalli, A. Fainstein, C. Vericat, M. E. Vela, R. C. Salvarezza, *J. Phys. Chem. C* **2008**, *112*, 3741.
[55] V. Zutic, V. Svetlicic, J. Clavilier, J. Chevalet, *J. Electroanal. Chem.* **1987**, *219*, 183.
[56] C. Vericat, F. R. Lenicov, S. Tanco, G. Andreasen, M. E. Vela, R. C. Salvarezza, *J. Phys. Chem. B* **2002**, *106*, 9114.
[57] T. Sagara, K. Niki, *Langmuir* **1993**, *9*, 831.
[58] S. H. A. Nicolai, J. C. Rubim, *Langmuir* **2003**, *19*, 4291.